

# Nanofabrication and characterization of ZnO nanorod arrays and branched microrods by aqueous solution route and rapid thermal processing

Oleg Lupan<sup>a,b,\*</sup>, Lee Chow<sup>a</sup>, Guangyu Chai<sup>c</sup>, Beatriz Roldan<sup>a</sup>,  
Ahmed Naitabdi<sup>a</sup>, Alfons Schulte<sup>a</sup>, Helge Heinrich<sup>a,d</sup>

<sup>a</sup> Department of Physics, University of Central Florida, P.O. Box 162385 Orlando, FL 32816-2385, USA

<sup>b</sup> Department of Microelectronics and Semiconductor Devices, Technical University of Moldova,  
168 Stefan cel Mare Boulevard, MD-2004 Chisinau, Republic of Moldova

<sup>c</sup> Apollo Technologies, Inc., 205 Waymont Court, S111, Lake Mary, FL 32746, USA

<sup>d</sup> Advanced Materials Processing and Analysis Center, and Department of Mechanical, Materials, and Aerospace Engineering,  
University of Central Florida, P.O. Box 162385, Orlando, FL 32816-2455, USA

Received 24 May 2007; received in revised form 2 October 2007; accepted 6 October 2007

## Abstract

This paper presents an inexpensive and fast fabrication method for one-dimensional (1D) ZnO nanorod arrays and branched two-dimensional (2D), three-dimensional (3D) – nanoarchitectures. Our synthesis technique includes the use of an aqueous solution route and post-growth rapid thermal annealing. It permits rapid and controlled growth of ZnO nanorod arrays of 1D – rods, 2D – crosses, and 3D – tetrapods without the use of templates or seeds. The obtained ZnO nanorods are uniformly distributed on the surface of Si substrates and individual or branched nano/microrods can be easily transferred to other substrates. Process parameters such as concentration, temperature and time, type of substrate and the reactor design are critical for the formation of nanorod arrays with thin diameter and transferable nanoarchitectures. X-ray diffraction, scanning electron microscopy, X-ray photoelectron spectroscopy, transmission electron microscopy and Micro-Raman spectroscopy have been used to characterize the samples.

© 2007 Elsevier B.V. All rights reserved.

**Keywords:** ZnO nanorod; Branched microrods; Nanofabrication; Transferable nanoarchitectures

## 1. Introduction

ZnO is a key functional material exhibiting near-ultraviolet emission, transparent conductivity, semiconducting, magnetic, and piezoelectric properties. It has a wide direct band gap (3.37 eV), large exciton binding energy (60 meV), excellent chemical, mechanical, and thermal stability, and biocompatibility [1,2]. Zinc oxide has extensive commercial use during the past 100 years [3], with important applications in optoelectronics, nano/microelectronics, sensors, transducers, and biomedicine.

Recently, one-dimensional (1D) zinc oxide materials and differently shaped ZnO nanocrystals have attracted considerable attention due to their unique properties that strongly depend on their size and morphologies [4] and their possible use as building blocks in near-future nanodevices [5,6]. 2D- and 3D-shaped ZnO nanocrystals will play a significant role as the novel functional units of electronic, electromechanical and optoelectronic devices [7–10], and nanosensors [5,6,11–13].

Novel synthesis routes of ZnO nanorods for solar cells and chemical sensing applications are currently being developed. The latest research efforts are directed towards obtaining alternative, lightweight, flexible nanodevices [14,15]. A number of publications address dye sensitized solid-state solar cells, which are currently the most stable and efficient excitonic solar cells for large-scale solar energy conversion [14,16–17]. In these cells, 1D ZnO nanorods with high carrier mobility can serve as direct conduction pathways for the excitons. The synthesis of a porous

\* Corresponding author. Tel.: +1 407 823 2333; fax: +1 407 823 5112.

E-mail addresses: lupanoleg@yahoo.com, lupan@physics.ucf.edu (O. Lupan).

structure with a high interfacial area is of primary importance for beneficial three-dimensional interpenetrating networks between the semiconductor/dye and the solid-state electrolyte. In the near future, it is expected that ZnO-based materials will supplant GaN in exciton polariton lasers, because exciton-stimulated emission and optically pumped lasing action in high-quality ZnO have been observed at room temperature [18–20].

Extensive effort is currently devoted to the controlled synthesis and characterization of ZnO nanostructures. Several different methods for the fabrication of ZnO nanorods and arrays have been reported, including hydrothermal synthesis [1,11], vapour–liquid–solid (VLS), vapour–solid (VS) [5] processes, metal–organic chemical vapor deposition (MOCVD) [14], chemical vapor deposition [21], solution–liquid–solid growth in organic solvents [22], and template-based methods [23–26].

Most reported synthesis techniques are complicated, time and energy consuming, and not environmentally friendly. In particular, when organo-metallic precursors are used, complex procedures, high temperatures and sophisticated equipment to control the growth process are involved [6,27].

For commercial use of ZnO nanorod arrays and individual nano/microrods for novel nano/microdevice applications, a simple, inexpensive and bio-safe synthesis process is required. Here, we report a novel synthesis route for ZnO nanorod arrays and branched nano/microrods, which overcomes the shortcomings of previous preparation methods. The growth of shape-controlled ZnO nanorod arrays in large scale is achieved in a zinc sulfate aqueous solution by adjusting composition, concentrations and growth temperature. Furthermore, the 1D, 2D and 3D nano/microrods obtained can be easily transferred to other substrates opening the possibility of studying the assembly of different functional units in novel nanodevices, nano/microrod p–n junctions, nanosensors and single crystal logic nanogates.

## 2. Experimental details

### 2.1. Synthesis

In the synthesis process, the amorphous glass or crystalline quartz substrates were first cleaned in a diluted HCl (20%) solution for 10 min and then rinsed in de-ionized (DI) water (~18.2 MΩ cm). Subsequently, the substrates were ultrasonically cleaned in an ethanol/acetone (1:1) mixture, then DI water, and dried in air. Solutions of SnCl<sub>2</sub>/HCl were used for the sensitization of the substrate surface. This cleaning procedure was found to be adequate for generating a uniformly wettable substrate surface. For silicon substrates, the standard procedure described in Ref. [28] was used to clean these substrate surfaces.

Zinc sulfate [Zn(SO<sub>4</sub>)·7H<sub>2</sub>O] and ammonia (NH<sub>4</sub>OH) (Fisher Scientific, reagent grade, without further purification) were used for the synthesis of ZnO nanoarchitectures. 0.1–0.15 M Zn(SO<sub>4</sub>)·7H<sub>2</sub>O and ammonia solution NH<sub>4</sub>OH (29.6%) were mixed with 100 ml DI–water until complete dissolution at room temperature and became colorless. The substrates were kept in a SnCl<sub>2</sub>/HCl solution for 3–5 min, and then rinsed with a jet of DI water. Finally, the glass, quartz, and Si substrates were placed inside an aqueous solution in a reactor. It consists

of a glass beaker (5 cm in diameter) with a sphericalconcave cap with the radius of curvature of the surface of 10 cm and an orifice (1 mm in radius) on the side. The setup was mounted on a hot plate, and the temperature was quickly increased to 90–95 °C and kept constant for 15 min without any stirring. Manipulation and reactions were carried out in air inside a fumehood. In our experiment, ZnO nanocrystals (samples #1.1, #2.1 and #3.1) were formed at a pH value of 10–11.

One set of samples (#3.1) was prepared using 0.1–0.5 M of Zn(SO<sub>4</sub>)·7H<sub>2</sub>O and 0.001–0.005 M of aluminum sulfate Al<sub>2</sub>(SO<sub>4</sub>)<sub>3</sub>·18H<sub>2</sub>O (99.7%) which was dissolved in 100 ml DI–water. An ammonia solution (29.6%) was added which immediately started a heterogeneous reaction in a reactor. It was placed on a hot plate 90–95 °C and deposition on the substrates occurred for 15 min. After the reaction, the whole system was left on the hot plate (turned off), and slowly cool off from 90 °C to 40 °C in 30 min. Finally, the substrates were rinsed in deionized water for 2 min and then the samples were dried in air at 150 °C for 5 min.

In order to investigate the effect of post-deposition annealing, the obtained nanoarchitectures were rapid thermal processed (RTP) at different temperatures from 300 to 850 °C in a forming gas ambient using an annealing furnace maintained at a specific temperature. The duration of RTP was 20–200 s and the temperature was 500–850 °C for ZnO, according to previous reports [29,30]. For the present ZnO nanoarchitectures the optimal duration was found to be 60–120 s, at temperatures of 650–750 °C. The ZnO processing details are summarized in Table 1.

### 2.2. Characterization

The as-prepared and rapid thermal processed ZnO nanorod arrays and microrods were characterized by X-ray diffraction (XRD) using a Rigaku ‘D/B max’ X-ray diffractometer equipped with a monochromatized Cu Kα radiation source (λ = 1.54178 Å). The operating conditions were 30 mA and 40 kV at a scanning rate of 0.02°/s in the 2θ range from 10 to 90°. Data acquisition was made with the software Data Scan 3.1 and analyzed with Jade 3.1 (from Materials Data Inc.). The composition and morphologies of ZnO films were characterized by Rutherford backscattering spectroscopy (RBS) using a General IONEX 1.7 MV Tandemron, Energy dispersive X-ray spectroscopy (EDX), in combination with scanning electron microscopy (SEM) is using a JEOL and a Hitachi S800. Transmission electron microscopy (TEM) images were performed with a FEI Tecnai F30 TEM at an accelerating voltage of 300 kV. The different characterization techniques confirmed that the nanorod arrays are highly crystalline with regular rods distributed throughout the substrate surface. This morphology is considered to play a vital role in nanodevice applications.

The ex-situ prepared samples were subsequently transferred into an ultrahigh vacuum system (UHV) for electronic/chemical characterization. All in-situ investigations were performed in a modular UHV system (SPECS GmbH) specially designed for the preparation and characterization of nanoscaled materials. The analysis chamber is equipped with a hemispherical electron energy analyzer (Phoibos 100) and dual-anode (Al Kα,

Table 1

The schedules of ZnO nanorod arrays and microrods for as-grown samples and after rapid thermal processing

RTP regimes	Sample					
	#1.1 ZnO/glass	#2.1 ZnO/quartz	#3.1 ZnO/Si	#1.2 ZnO/glass	#2.2 ZnO/quartz	#3.2 ZnO/Si
Duration (s)	As grown	As grown	As grown	120	120	120
Temperature (°C)	–	–	–	650	650	650

1486.6 eV and Ag L $\alpha$ , 2984.4 eV) monochromatic X-ray source (XR50, SPECS GmbH) for X-ray photoelectron spectroscopy (XPS). The base pressure in this chamber is  $1\text{--}2 \times 10^{-10}$  mbar. In our studies, Al K $\alpha$  radiation was used.

Micro-Raman scattering experiments were performed with a Horiba Jobin Yvon LabRam IR system at a spatial resolution of  $2 \mu\text{m}$  in a backscattering configuration. The 633 nm line of a Helium Neon laser was used for off-resonance excitation with less than 4 mW of power at the sample. The spectral resolution was  $2 \text{cm}^{-1}$ , and the instrument was calibrated to the same accuracy using a naphthalene standard.

### 3. Results and discussion

#### 3.1. Structural and morphological-characterization (XRD, SEM, TEM) of ZnO nanoarchitectures

Fig. 1 shows the XRD pattern recorded in the range of  $15\text{--}90^\circ$  with a scanning step of  $0.02^\circ$  of ZnO nanoarchitectures before and after RTP. It can be seen that all diffraction peaks are caused by crystalline ZnO with the hexagonal wurtzite structure (space group:  $P6_3mc(186)$ ;  $a = 0.3249 \text{ nm}$ ,  $c = 0.5206 \text{ nm}$ ). The data are in agreement with the Joint Committee on Powder Diffraction Standards (JCPDS) card for ZnO (JCPDS 036–1451) [31].

No characteristic peaks of impurity phases such as Zn, S or  $\text{Zn}(\text{OH})_2$  are observed, and no diffraction peaks except ZnO were found, which indicates that only single-phase hexagonal ZnO is present. The ZnO nanocrystallites on glass (sample #1.1) are oriented along the  $c$ -axis in the (002) direction (Fig. 1a). No modification of the ZnO crystal structure was observed. The sharp diffraction peaks demonstrate that the as-synthesized ZnO nanorods have high crystallinity. The relative intensity of the ZnO (002) peak compared to the other ZnO peak intensities is higher than expected for bulk ZnO, indicating a preferential growth of nanorods on glass substrate in the (0001) orientation. This texture shows that as-grown ZnO (sample #1.1) is a 1D structure (Fig. 1(a)). The impact of the rapid thermal processing on the XRD pattern and surface morphology of the deposited nanoarchitectures has also been investigated. In the  $300\text{--}550^\circ\text{C}$  temperature ranges the films' XRD pattern and surface morphology did not differ from that of the as-grown ZnO (see Fig. 1). In the  $600\text{--}750^\circ\text{C}$  range the widths of the Bragg peaks became sharper for sample #1.2, but not for samples #2.2 or #3.2. For annealing temperatures higher than  $800^\circ\text{C}$  the edges of the ZnO nanorods start to melt.

In Fig. 1(a), the strongest detected ( $hkl$ ) peaks are at  $2\theta$  values of  $31.7^\circ$ ,  $34.4^\circ$ ,  $36.2^\circ$ ,  $47.5^\circ$ ,  $56.6^\circ$ , and  $62.8^\circ$ , corresponding to the following lattice planes: (100), (002), (101),

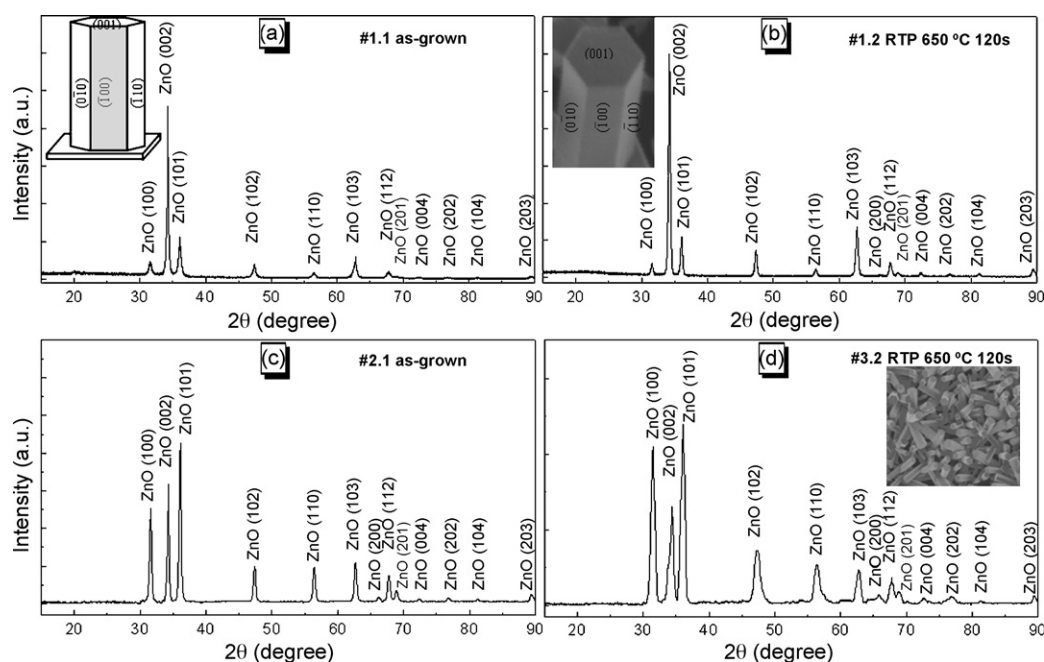


Fig. 1. XRD pattern of ZnO nanorods: (a) arrays as-prepared on glass (sample #1.1) and (b) arrays on glass after RTP (sample #1.2); (c) as-prepared nanorods and microrods on quartz (sample #2.1) and (d) nanorod and microrods on Si after RTP at  $650^\circ\text{C}$  for 120 s (sample #3.2) synthesized by the aqueous-solution method. The inset is SEM images of ZnO nanorod and nanorod arrays.

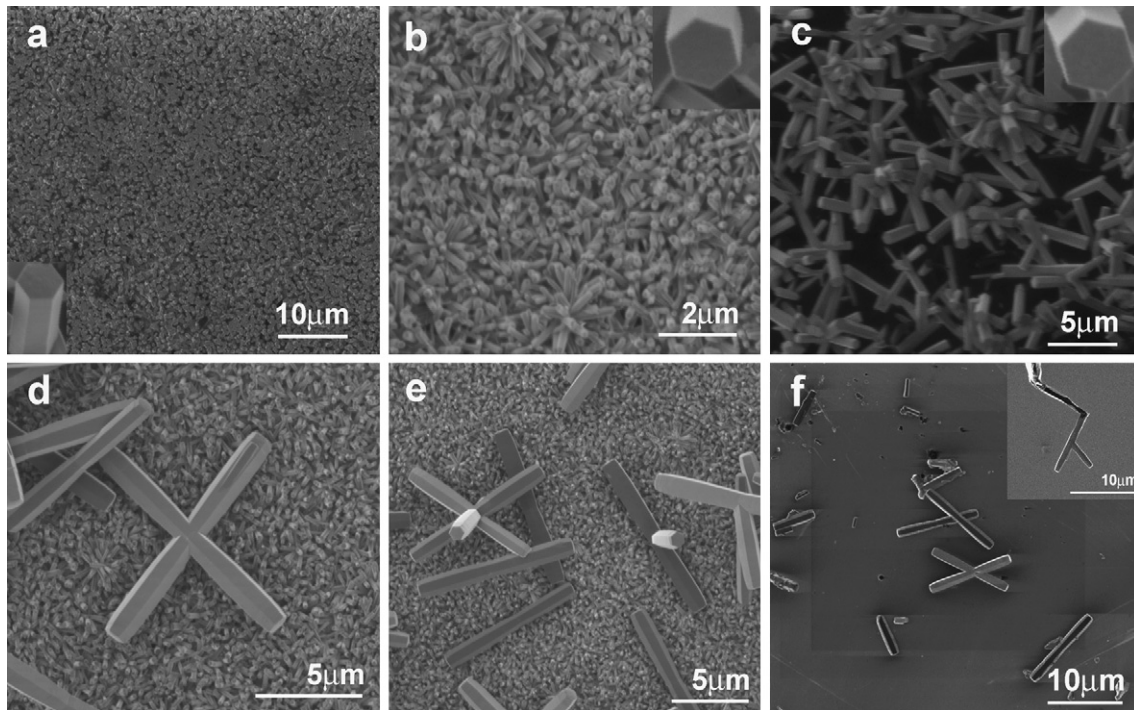


Fig. 2. The SEM images of the ZnO nanorods chemically grown from ZnSO<sub>4</sub> and ammonia aqueous bath on (a) glass substrates (samples #1.1 and #1.2) and inset hexagonal rod images; (b) on quartz substrates (samples #2.1 and #2.2), and (c) Si substrates (samples #3.1 and #3.2); The insets in Fig. 2(a)–(c) display single ZnO rods with hexagonal basis. Image (d) corresponds to two-dimensional 2D ZnO crosses, (e) to branched 1D, 2D, and 3D microrods with ZnO nanorod arrays as background, and (f) to 1D and 2D branched microrods transferred to another Si substrate, The insert in (f) the right-up corner shows an individual tripod picked-up the in-situ lift-out needle in the focused ion beam (FIB) system.

(102), (110), (103), respectively. The lattice constants  $a$  and  $c$  were determined as  $a = 0.3249$  nm,  $c = 0.5206$  nm by using the following equation [32]

$$\frac{1}{d_{(hkl)}^2} = \frac{4}{3} \left( \frac{h^2 + hk + k^2}{a^2} \right) + \frac{l^2}{c^2}. \quad (1)$$

The intensity of the peaks relative to the background signal demonstrates high purity of the hexagonal ZnO phase and good crystallinity of the samples. The XRD pattern (Fig. 1(a) and (b)) indicate a (002)-preferred orientation, which suggests that the rods are quasi-aligned with the optical  $c$ -axis which is oriented perpendicularly to the substrate surface. The texture coefficient for the (002) orientation is estimated to be about 3.2 from the following relation [33]:

$$TC_{(002)} = \frac{I_{(002)}/I_{(002)}^0}{(1/N) \sum I_{(hkl)}/I_{(hkl)}^0}, \quad (2)$$

where  $N$  is the number of diffraction peaks, and  $I_{(hkl)}$  and  $I_{(hkl)}^0$  are the measured and corresponding recorded intensities according to the JCPDS 036-1451 card [31]. This value is comparable with the one inherent to the best ZnO nanorod samples [33].

In samples #1.1 and #1.2 the strongest peak corresponds to the (002) direction. The (101) peak was the strongest for samples #2.1, #2.2, #3.1 and #3.2. This observation indicated that (101) crystal planes were more prevalent for the nanostructures on quartz and Si.

In order to examine the surface morphology and for measurement of the rod sizes, SEM has been used. Typical SEM images

of the ZnO nanorod arrays and individual microrods are shown in Fig. 2. The overall morphology of the ZnO nanorod arrays on a glass substrate is shown in Fig. 2(a), which indicates the obtained product consist of nanorods with an average diameter of 300 nm. The lengths of ZnO nanorods are about 2 μm. ZnO nanorods with diameters of 100 nm have also been synthesized on quartz with this method (Fig. 2(b)). The morphology of the ZnO nanorods grown on Si is shown in Fig. 2(c). The SEM images of ZnO samples after RTP at 650–750 °C do not differ from those shown in Fig. 2(a)–(c). New 1D, 2D and 3D ZnO branched microrods are presented in Fig. 2(d)–(f). According to our experimental results, the branched architectures obtained by our process can be easily transferred to other substrates and handled by focused ion beam FIB in order to fabricate different nanodevices (Fig. 2(f)). The insert in Fig. 2(f) the right-up corner shows an individual tripod picked-up the in-situ lift-out needle in the focused ion beam system. The inserts in Fig. 2(a)–(c) correspond to high-resolution SEM images taken on single rods, and display the hexagonal base of our nanorods on different substrates.

The analysis of Fig. 2(c) reveals that each individual ZnO nanorod has a hexagonal shape with a diameter of about 300 nm and a length of about 5 μm. (This rod was found on a sample grown in 45 min on a Si substrate.)

After experiments with aluminum sulfate in solution and quartz substrate and Si substrate we observed that nanorods growth similarly with a difference only in their quantity per unit of area. For example, Si substrate showed the lowest density of deposited ZnO nanorods, presumably due to a much perfect surface than that of the quartz substrate. In experiments without

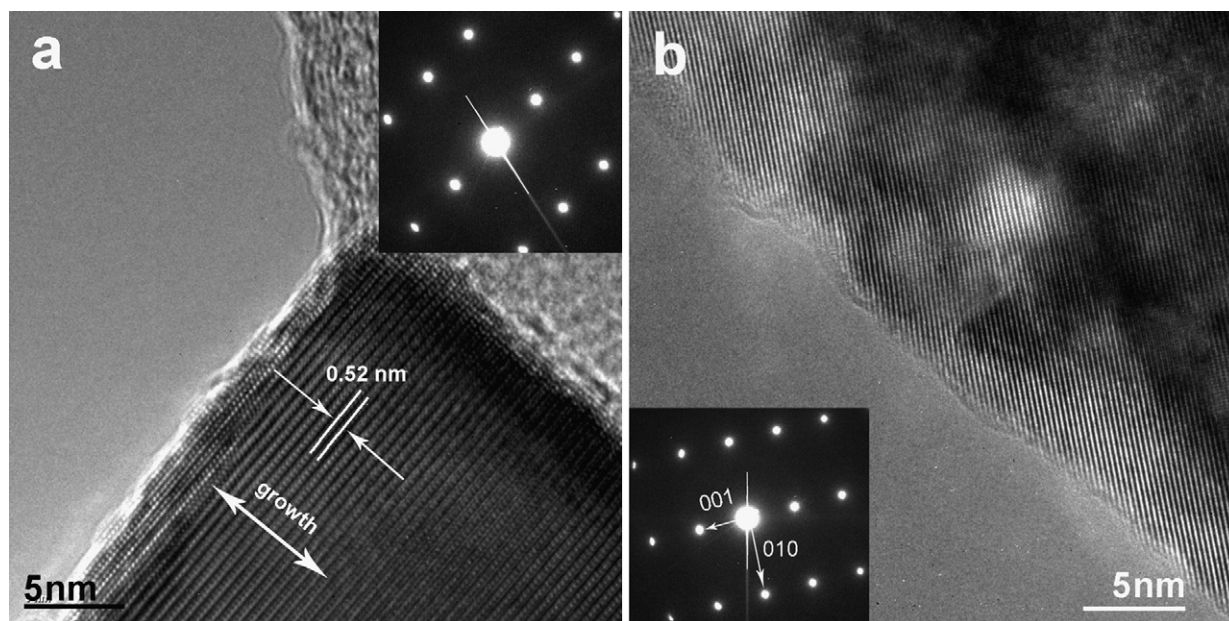


Fig. 3. The High-resolution TEM images and the inset with the select area diffraction patterns of the single-crystalline ZnO nanorods (sample #2.1) grown by aqueous solution deposition. The diffraction patterns show that the nanorod grows along the (0001) direction.

using aluminum sulfate in solution, it was observed that similar nanorods growth on quartz substrate and Si substrate.

Transmission electron microscopy was employed to characterize the as-synthesized ZnO nanorods, and to observe the nanostructure. To prepare TEM samples, the nanorods were scraped from the substrate onto an amorphous holey carbon film covered copper grid. Alternatively, they were transferred and mounted on the inside of a TEM Cu-ring by the in-situ lift-out technique in a FIB system.

The corresponding TEM images and selective area electron diffraction (SAED) pattern of individual ZnO nanorod (sample #2.1) are shown in Fig. 3. As indexed (Fig. 3(b)) in the down-right corner of the inset SAED pattern, the nanorod is grown along the direction of (001) zone axis of ZnO, which corresponds with the HRTEM result. The incident beam is along the zone axis. For the samples #1.1, #1.2, #3.1 and #3.2 similar HRTEM results and SAED patterns have been observed.

The TEM images indicate that the entire as-grown ZnO nanorod is single-crystalline ZnO with a wurtzite structure grown along the (001) direction, which is consistent with the XRD results. The HRTEM lattice fringes and SAED patterns shown in Fig. 3 reveal that, in this region, the nanorods possess a single crystal hexagonal structure without dislocations and stacking faults. The micrograph also confirms that the nanorods grow along the (001) direction (indicated with an arrow). With TEM characterization we found that nanorods and branched microrods are not bent with a smooth surface.

Using energy dispersion X-ray spectroscopy (EDX) and Rutherford back scattering (RBS), the formation of the ZnO was confirmed. The Zn:O ratios in our nanostructures were analyzed by RBS and EDX measurement and were found to be 1:1 atomic ratio in all samples. The quality of the grown ZnO rods is demonstrated by the stoichiometric composition deduced from the RBS and EDX analysis as well as by the XRD crystallographic data.

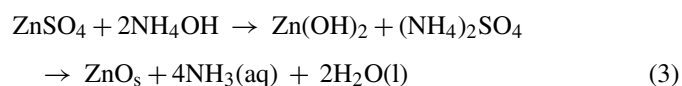
The effect of the rapid thermal processing on the surface morphology of the synthesized nanoarchitectures has also been investigated. In the 100–700 °C temperature range, the film's surface morphology does not differ from that of the as-grown ZnO (see Fig. 2). According to our observations, the ZnO nanorods maintain their rod-like morphology till 800–850 °C.

### 3.2. Growth mechanism of ZnO branched nanorods

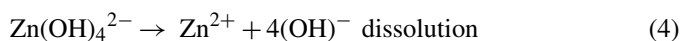
Next, the growth mechanism of ZnO one-dimensional and branched nanorods in aqueous solution of zinc sulfate and ammonia is discussed. The reason behind this preferred crystallization can be understood by considering that ZnO wurtzite crystals have different growth rates for different planes:  $V_{(0001)} > V_{(10\bar{1}1)} > V_{(10\bar{1}0)}$ . Because of these different growth rates, the controlled synthesis of preferred nanoarchitecture for specific applications can be realized. The crystal synthesis on a specific surface in the aqueous solution is based on heterogeneous nucleation and subsequent growth.

Due to the fact that the heterogeneous nucleation takes place at a low level of supersaturation of the complex solution, we can grow different ZnO nanoarchitectures (Fig. 2) by controlling the reactant concentration, process temperature, and pH value.

The global reaction for ZnO crystal growth by aqueous solution deposition is



According to our experimental observation the growth of ZnO nanorods in aqueous solution can be explained as follows: As the temperature increases the following reactions occur.



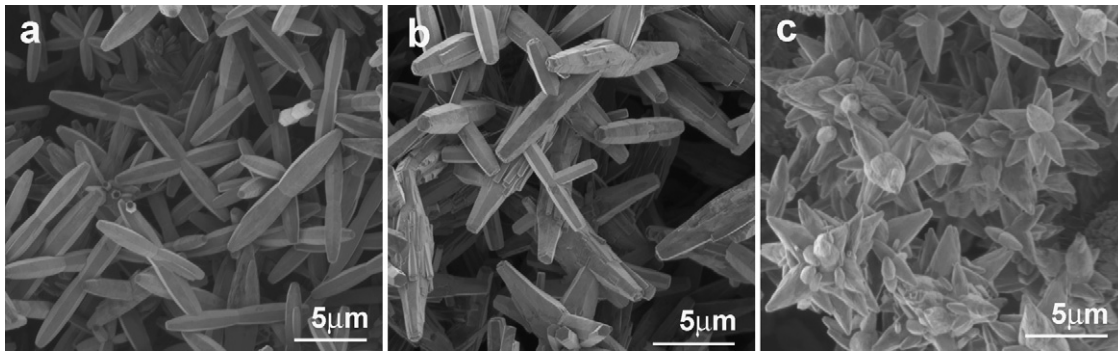
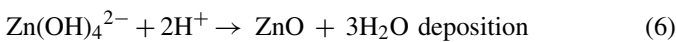
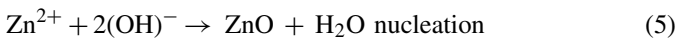


Fig. 4. The SEM images of the branched and flower-like ZnO nanorods chemically grown from a zinc sulfate and an ammonia aqueous bath: (a) two-step routes ZnO on a Si substrate; (b) in three-step routes ZnO on quartz and Si; (c) in one-step routes of the homogeneous reaction ZnO on quartz and Si.



When the concentration of  $\text{Zn}^{2+}$  and  $\text{OH}^{-}$  exceed supersaturation, ZnO nuclei are formed on the substrate surface.

With increasing temperature these complexes become dehydrated and heterogeneous nucleation of ZnO crystals takes place at the interface between substrate and solution. After that, the crystals will grow into nanorods. The  $\text{Zn}(\text{OH})_4^{2-}$  ions decompose to produce ZnO molecular species [34] which form seeds and grow to form hexagonal nucleus and finally individual one-dimensional nanorods and branched nanorod.

According to our experimental results and detailed cross-section investigation have not been observed ZnO film growth before the formation of nanorods/nanowires. Thus we can conclude that nanorods/nanowires started to grow from formed ZnO hexagonal nuclei on the substrate surface. The reason of ZnO nanorods growth in 10–15 min of reaction can be explained by higher-symmetry ( $C_{6v}$ ) for plane (001) than other faces, respectively highest growth rates along  $+c$  axis. Thus, the controlled synthesis of 1D nanoarchitectures can be realized by altering  $\text{Zn}^{2+}/\text{OH}^{-}$  ratio (see relations (4)–(6)) and use different substrates. Also offer possibility to grow transferable nanorods. This easy transfer of ZnO architectures to any substrate and pick-up by in-situ lift-out FIB, opening the possibility of reproducibly nanofabrication and studying novel nanodevices.

In the case for  $\text{Zn}^{2+}/\text{OH}^{-}$  ratio of 1:2, wurtzite ZnO crystal zinc terminated (001) planes, which are active and promote 1D growth [35]. One face of the hexagonal sheet is Zn rich and forms (001) planes, while the opposite face is the (00 $\bar{1}$ ) plane. The ZnO nanocrystals are polar in nature, and the Zn-rich positive (001) surface is more reactive than the oxygen-rich negative (00 $\bar{1}$ ) surface and attracting new ZnO species to the surface and promoting anisotropic growth along the (001) direction [35].

Increasing the temperature of the zinc complex solution promotes dissociations, leading to a controlled supersaturation of the free  $\text{Zn}^{2+}$  ion. Experimental results confirm the possibility to tailor morphologies of ZnO nanoarchitectures by limiting the concentration of zinc ions or hydroxide, in the presence of the other. The size of ZnO nanorods is tuned by modifying the solution conditions – precursor concentration, catalyst type,

reaction time and temperature. Based on the “lowest-energy” theory [37] that dictates the preferred growing direction, the growth mechanism can be explained.

In Fig. 2, we measure an average diameter of the ZnO nanorods are  $\sim 100$  nm on quartz and  $\sim 300$  nm on glass substrates. The average length of ZnO nanorods in samples #1.1, #2.1, and #3.1, are 1  $\mu\text{m}$ , 0.5  $\mu\text{m}$ , and 4  $\mu\text{m}$ , respectively. In our experiments, the diameter of ZnO nanorods was found to be proportional to this concentration of reactant, while the nanorod length was inversely proportional to the concentration of the reactant, in agreement with previous observations by Vayssieres [36]. We observed that the shapes and the sizes of the ZnO nanorods are functions of duration, temperature and the solution concentration of reactants.

ZnO nanoarchitectures synthesized with a two-step heterogeneous reaction are shown in Fig. 4(a). Fig. 4(b) represents the microstructure for a three-step heterogeneous reaction, and Fig. 4(c) is a SEM micrograph of structures from a one-step homogeneous reaction.

According to our observations, the growth of branched rods on the ZnO nanorods during the two- and three-step processes (see Fig. 4) is not due to the lateral growth of the crystals, since this process is suppressed, while the growth along  $c$ -axis is dominant. In the two-step aqueous solution process occurring at the lowest concentrations, the ZnO crystal growth primarily proceed on the branched seed-crystals, consequently, the ZnO nanorods, which are (0001) oriented, eventually form on sides of the rods (see Fig. 2(c) and (d)). As was explained above, the precursor solution contained,  $\text{Zn}(\text{OH})_4^{2-}$  ions, which are supposed to be actively involved in the formation of nanorods.  $\text{Zn}(\text{OH})_4^{2-}$  species can act as the building blocks which are incorporated into the crystal lattice by a dehydration reaction. After a synthesis process of 15 min, the concentration of  $\text{Zn}(\text{OH})_4^{2-}$  significantly decreased due to its consumption by the growth of ZnO nanorods, thus, there was no elongation of ZnO nanorods in the subsequent process. The remaining  $\text{Zn}(\text{OH})_4^{2-}$  can be continuously incorporated into the crystal lattice on the nucleus formed on previously grown nanorods, thus, new ZnO crystallites grow along the  $c$ -axis with the fastest growth rate, while the lateral growth is sluggish due to the very low concentration of Zn source. Therefore, new ZnO nanorods with smaller diameters are formed on the flat planes of ZnO rods as a result of selective

epitaxy. This opens the possibility of growing nano/micro p–n junctions for novel nanodevices.

Alignment of the grown nanowires can be realized using specific template. Simplest way used to make ordered nanowire arrays during the growth is to create on the surface equal conditions to form seeds and to form uniformly distributed nucleus and finally nanorods.

### 3.3. Micro-Raman scattering

Another effective approach to investigate the phase and purity of the nanostructures grown is Raman scattering. Room temperature Micro-Raman spectroscopy was performed to examine the optical properties of these regular ZnO nanocrystal arrays. ZnO has a wurtzite structure and belongs to the  $C_{6V}^4$  space group or 6 mm symmetry [38]. The different symmetries involved govern whether vibrations are Raman active and appear in the spectra, while changes in lattice spacing and chemical environment may shift the vibrational frequencies. Therefore, we investigate the phase and purity of grown nanoarchitectures by study of Raman spectra. From group theory the following optical modes are predicted –  $A_1 + 2B_1 + E_1 + 2E_2$  at the  $\Gamma$  point of the Brillouin zone;  $B_1$  (low) and  $B_1$  (high) modes are normally silent;  $A_1$ ,  $E_1$ , and  $E_2$  modes are Raman active; and  $A_1$  and  $E_1$  are also infrared active and split into longitudinal (LO) and transverse (TO) optical components [39].

Representative Micro-Raman spectra of the ZnO nanorod arrays and 1D, 2D and 3D nanocrystals are shown in Fig. 5. When considering the wurtzite type ZnO (space group  $P6_3mc$ ), phonon modes  $E_2$  (low and high frequency),  $A_1$  (TO-transversal acoustic mode and LO-longitudinal optical components) and  $E_1$  (TO and LO) are expected. The high frequency  $E_2$  (high) mode is

clearly visible at  $438\text{ cm}^{-1}$  with a width of  $10\text{ cm}^{-1}$ , indicating the good crystal quality [40,41]. The smaller peak at  $332\text{ cm}^{-1}$  has been attributed to a second order  $E_2$  mode [38].

Due to propagation of  $E_1$  (LO) parallel to the  $(0\bar{1}1)$  direction is neither the XY-plane nor the Z-axis [39] in the backscattering configuration, the  $E_1$  (LO) mode near  $586\text{ cm}^{-1}$  cannot be observed from the vertically aligned nanorods (sample #1.1 and #1.2), but can be observed from the tilted microrods and randomly oriented nanorods (#3.1).

The Raman peaks at  $382$  and  $407\text{ cm}^{-1}$  can be assigned to the  $A_1$  mode and  $E_1$  mode of ZnO, respectively. The strong Raman peak at  $438\text{ cm}^{-1}$  was one of the characteristic peaks of wurtzite ZnO attributed to the  $E_2$  mode [40,41].

There are no significant differences between the measured spectra for different structures (1D, 2D and 3D) rods for samples #1.1 and #2.1 both in spectral position or intensity. Dominant peaks at  $100\text{ cm}^{-1}$  and  $438\text{ cm}^{-1}$ , which are commonly detected in the wurtzite structure ZnO [42], are attributed to the low- and high- $E_2$  mode of non-polar optical phonons, respectively. Two smaller peaks at  $332\text{ cm}^{-1}$  and  $382\text{ cm}^{-1}$  correspond to  $E_{2H}$ – $E_{2L}$  (multi phonon) and  $A_{1T}$  modes, respectively. The peak at  $578\text{ cm}^{-1}$  (Fig. 5(c)) is assigned to the  $E_{1L}$  mode due to impurities and structural defects (oxygen vacancies and Zn interstitials) [43]. The micro-Raman spectra of the investigated ZnO nanorod arrays and microrods depend on the collecting configuration and the crystal face.

### 3.4. Chemical characterization (XPS)

XPS was used to monitor changes in the chemical composition of the nanorods after two thermal treatments at  $150^\circ\text{C}$  (samples #1.1 and #3.1), and RTP at  $650^\circ\text{C}$  (samples #1.2 and

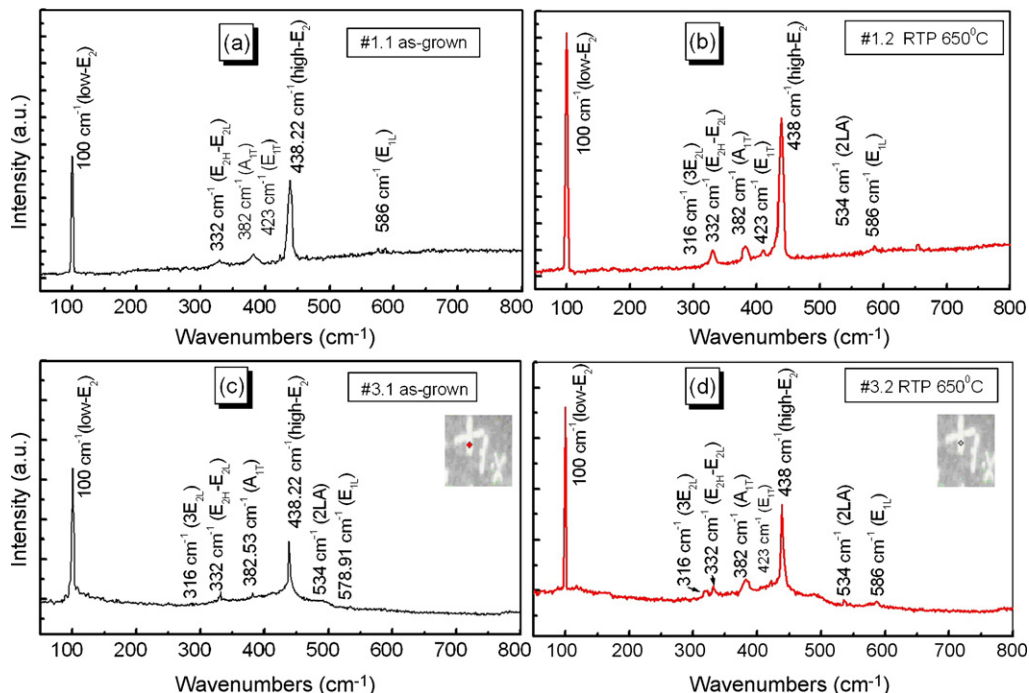


Fig. 5. Micro-Raman scattering spectra of: (a) the as-grown ZnO nanorod arrays, (b) RTP ZnO nanorod arrays, (c) as-grown cross microrods with hexagonal form and (d) RTP cross branched microrods with hexagonal form.

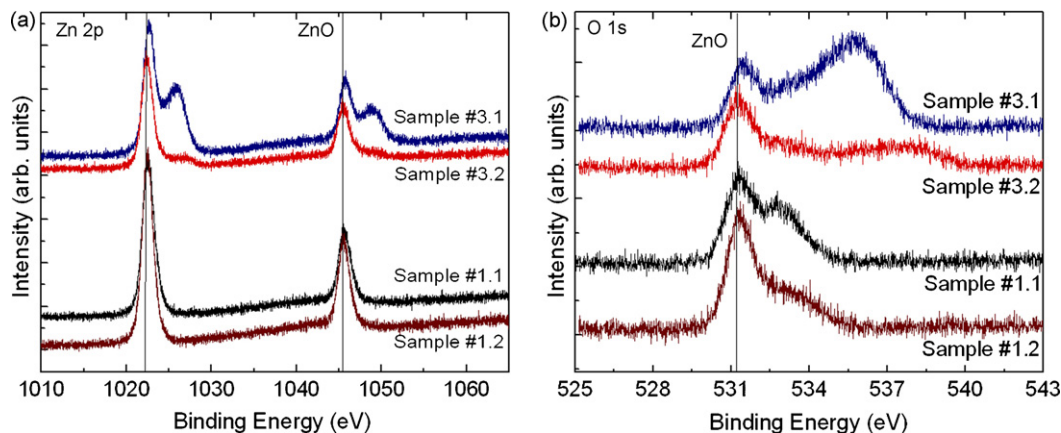


Fig. 6. XPS spectra (Al  $K\alpha=1486.6$  eV) corresponding to the (a) Zn-2p and (b) O-1s core levels of ZnO nanorods supported on glass and measured at room temperature after annealing in air at  $150^\circ\text{C}$  for  $\sim 3$  min (samples #1.1 and #3.1) and rapid thermal processed at  $650^\circ\text{C}$  for 120 s (samples #1.2 and #3.2).

#3.2). Fig. 6 shows XPS spectra from the Zn-2p (a) and O-1s (b) core level regions. Charging effects due to the low conductivity of the glass slides used as substrates have been minimized by calibrating the binding energy (BE) scale using the O-1s XPS peaks of ZnO (531.2 eV) and C-1s (285 eV) as references. A residual amount of adventitious C was detected in samples #1.1, #1.2 and #3.2, since they were measured after several days of air exposure. Sample #3.1 however was measured immediately after deposition, and no C-1s signal was found by XPS.

In Fig. 6(a), all samples show XPS peaks at  $\sim 1022.5$  eV and  $\sim 1045.5$  eV, corresponding to the  $2p_{3/2}$  and  $2p_{1/2}$  core levels of Zn in ZnO [44]. However, sample #3.1 shows two additional peaks at higher binding energies ( $\sim 1026$  eV and  $\sim 1049$  eV). The contribution of these peaks to the XPS spectrum is strongly reduced upon rapid thermal processing sample #3.1 at a higher temperature ( $650^\circ\text{C}$ ) as can be seen for sample #3.2. Since the spin-orbit split of this core level is analogous to what is found for ZnO ( $\sim 23$  eV), we attribute these new spectral features to a Zn-containing compound. Mar et al. [45] reported similar BEs (1026.3 eV for Zn  $2p_{3/2}$ ) for zinc acetate dehydrate [ $\text{ZnO}(\text{CH}_3\text{CO}_2)_2 \cdot 2\text{H}_2\text{O}$ ], and showed that it could be completely decomposed to ZnO upon sample annealing to  $350^\circ\text{C}$ . We cannot attribute our additional XPS peaks to the same compound, since in our case  $\text{ZnSO}_4$  was used as precursor for the nanowire growth, and no C-signal was detected for sample #3.1. We tentatively attribute our unstable Zn-compound (readily decomposed upon annealing to  $650^\circ\text{C}$ )  $\text{ZnSO}_4$  ( $\sim 1023$  eV) [46] from the sample preparation method, and the large BE shift observed to the reduced dimension of the ZnO rods, as well as to the presence of Al-doping. No significant changes in the Zn-2p core levels were found for the pure (undoped) ZnO samples upon annealing at  $150^\circ\text{C}$  (sample #1.1) and  $650^\circ\text{C}$  (sample #1.2).

In Fig. 6(b), all samples show a clear photoelectron peak at  $\sim 531.2$  eV, corresponding to the O 1s core level in ZnO [47]. A second peak at 535.8 eV is observed for the sample (labeled #3.1) doped with Al after annealing at  $150^\circ\text{C}$ . After rapid thermal processing the same sample to  $650^\circ\text{C}$  (sample #3.2), the intensity of the second peak was strongly reduced, and it shifted to 537.7 eV. Pashutski et al. [48] reported similar high O-1s binding energies for  $\text{N}_2\text{O}$  (535.6 eV) and NO (536.2 eV) adsorbed

on Al. Hydroxide groups are also known to display XPS features at 535.1 eV [49] and 538 eV [50] binding energies. Because  $\text{ZnSO}_4$ ,  $\text{NH}_4\text{OH}$  and  $\text{Al}_2(\text{SO}_4)_3$  were used as precursors for the nanorod growth, both options can explain the observed XPS signatures. However, since the analogously prepared undoped samples (#1.1 and #1.2) did not show such peaks, we attribute them to the presence of the Al doping. In addition, sample #3.2 also shows a shoulder at  $\sim 533$  eV [51]. The same feature appears in the two undoped samples (at 532.9 eV in sample #1.1 and 533.4 eV in sample #1.2). Similar BEs have been attributed to O-1s in  $\text{SiO}_2$  (533 eV) [52], to oxidic species located at the surface of ZnO films ( $+1.8$  eV shifted with respect to O-1s in bulk-like ZnO) [53], and to hydroxide species [53]. Although it is possible to measure a residual  $\text{SiO}_2$  signal from the glass substrate used by XPS (thin ZnO rod coverage), due to the high thermal stability of  $\text{SiO}_2$  ( $\sim 1000^\circ\text{C}$ ), this signal should not be significantly modified by the RTP at  $650^\circ\text{C}$ . This is in contrast to our observations for samples #1.1 and #1.2, where the high BE peak is suppressed upon RTP. Because of the sample preparation method used, the presence of hydroxide species cannot be ruled out. However, it must be noted that analogous high energy O-1s XPS features have also been observed on ZnO single crystals [53] and attributed to surface oxide species.

#### 4. Conclusion

In summary, thin and thick ZnO nanorods arrays, single nanorods and one-, two-, three-dimensional-branched microrods were synthesized through a novel low-temperature aqueous solution route and rapid thermal processing. ZnO nanorods and branched microrods are found to have high crystal quality with *c*-axis orientation. Each individual ZnO rod showed a hexagonal basis and its dimensions was found to depend on synthesis and process parameters such as concentration, temperature and time, type of substrate and the reactor design. Rapid thermal processing permits an overall improvement of the crystal quality and allows the control of the properties of nanorod arrays.

In this investigation, ZnO nanoarchitectures deposited on glass, quartz and Si substrates were synthesized using an aqueous solution method without the need of catalysts, templates,

or seeds. The nanofabrication route used in this study differs from the ordinary aqueous solution route, but shows much better results in terms of growth rate of the ZnO nanorod arrays and branched 1D, 2D and 3D nano/microrods architectures. This work also showed a method for an easy transfer of synthesized ZnO architectures to any substrate and pick-up by using in-situ lift-out FIB, opening the possibility of reproducibly fabrication and studying novel nanodevices.

X-ray diffraction, scanning electron microscopy, high-resolution transmission electron microscopy, X-ray photoelectron spectroscopy and micro-Raman spectroscopy have been used to characterize the structure, morphology and chemical composition of the samples. The ZnO rods synthesized here were found to be of single-crystal nature with hexagonal wurtzite structure and stoichiometric ZnO composition. Further, they presented high crystal quality and narrow diameter distributions. XRD and SAED measurements indicate that the synthesized ZnO crystals are in the hexagonal phase and well-aligned parallel to the (0001) crystal direction.

The growth morphology and growth mechanism, as well as crystalline quality of individual microrods have been carefully investigated by SEM, TEM, and micro-Raman. We observe a uniform distribution of diameters of the rods for ZnO on a glass substrate. SEM and high-resolution TEM images show that the nanorods' growth can be completed in 15 min and regulated by growth parameters. The main advantage of the proposed synthesis is its simplicity and fast growth rates (15 min versus several hours reported by previous researchers using aqueous synthesis methods or others). The strength of the proposed nanotechnology is that any substrate can be used to grow ZnO nanorods and individual 2D, 3D-branched rods. According to our experience, it is envisioned that p–n nanorods-based p–n junctions can be fabricated using presented nanotechnology.

Further work on the optimization of pure and doped ZnO nanorod growth for electronic and optoelectronic device applications are in progress. It is anticipated that the ZnO branched rods will find many applications in novel nanodevices [54] and are expected to promote synthesis of nanorod p–n junctions.

## Acknowledgments

The research described here was made possible in part by an Award (MTFP-1014B) and Project MOE2-3052-CS-03 from the Moldovan Research and Development Association (MRDA) under funding from the U.S. Civilian Research & Development Foundation (CRDF). The financial supports by the Ministry of Education and Science of R. Moldova through the Project 321b/s are gratefully acknowledged. This work was also partially supported by the National Science Foundation (NSF-CAREER award No. 0448491) and DMR-0421253 and the Donors of the American Chemical Society Petroleum Research Fund under Grant PRF-42701-G5.

## References

- [1] T. Ma, M. Guo, M. Zhang, Y. Zhang, X. Wang, *Nanotechnology* 18 (2007) 035605.
- [2] Ü. Özgür, Ya.I. Alivov, C. Liu, A. Teke, M.A. Reshchikov, S. Dogan, V. Avrutin, S.J. Cho, H. Morkoç, *J. Appl. Phys.* 98 (2005) 041301.
- [3] T. Ghoshal, S. Kar, S. Chaudhuri, *J. Cryst. Growth* 293 (2006) 438.
- [4] J.Y. Chen, T. Herricks, Y.N. Xia, *Angew. Chem., Int. Ed.* 44 (2005) 2589.
- [5] G.C. Yi, C. Wang, W. Park, *Semicond. Sci. Technol.* 20 (2005) S22.
- [6] Z.P. Sun, L. Liu, L. Zhang, D.Z. Jia, *Nanotechnology* 17 (2006) 2266.
- [7] J.C. Johnson, H. Yan, R.D. Schaller, L.H. Haber, R.J. Saykally, P. Yang, *J. Phys. Chem. B* 105 (46) (2001) 11387.
- [8] J.B.K. Law, J.T.L. Thong, *Appl. Phys. Lett.* 88 (2006) 133114.
- [9] R. Hauschild, H. Kalt, *Appl. Phys. Lett.* 89 (2006) 123107.
- [10] M.H. Huang, S. Mao, *Science* 292 (2001) 1897.
- [11] J.X. Wang, X.W. Sun, Y. Yang, H. Huang, Y.C. Lee, O.K. Tan, L. Vayssieres, *Nanotechnology* 17 (2006) 4995.
- [12] P.S. Cho, *J. Electroceram.* 17 (2006) 975.
- [13] M.C. Newton, S. Firth, P.A. Warburton, *Appl. Phys. Lett.* 89 (2006) 072104.
- [14] E. Galoppini, J. Rochford, H. Chen, G. Saraf, Y. Lu, A. Hagfeldt, G. Boschloo, *J. Phys. Chem. B* 110 (2006) 16159.
- [15] A.D. Pasquier, H. Chen, Y. Lu, *Appl. Phys. Lett.* 89 (2006) 253513.
- [16] M. Law, L.E. Greene, J.C. Johnson, R. Saykally, P. Yang, *Nat. Mater.* 4 (2005) 455.
- [17] B.A. Gregg, *J. Phys. Chem. B* 107 (2003) 4688.
- [18] P. Zu, Z.K. Tang, G.K.L. Wong, M. Kawasaki, A. Ohtomo, H. Koinuma, Y. Segawa, *Solid State Commun.* 103 (1997) 459.
- [19] D.M. Bagnall, Y.F. Chen, Z. Zhu, T. Yao, S. Koyama, M.Y. Shen, T. Goto, *Appl. Phys. Lett.* 70 (1997) 2230.
- [20] H.M. Cheng, H.C. Hsu, S. Yang, C.Y. Wu, Y.C. Lee, L.J. Lin, W.F. Hsieh, *Nanotechnology* 16 (2005) 2882.
- [21] J.J. Wu, S.C. Liu, *Adv. Mater.* 14 (2003) 215.
- [22] W.T. Yao, S.H. Yu, *Int. J. Nanotechnol.* 4 (2007) 129.
- [23] Y. Li, G.W. Meng, L.D. Zhang, *Appl. Phys. Lett.* 76 (2000) 2011.
- [24] C.L. Hsu, S.J. Chang, H.C. Hung, Y.R. Lin, C.J. Huang, Y.K. Tseng, I.C. Chen, *IEEE Trans. Nanotechnol.* 4 (2005) 649.
- [25] Y. Li, G.W. Meng, L.D. Zhang, F. Phillipp, *Appl. Phys. Lett.* 76 (2000) 2011.
- [26] S.H. Park, S.H. Kim, S.W. Han, *Nanotechnology* 18 (2007) 055608.
- [27] M. Guo, P. Diao, X. Wang, S. Cai, *J. Solid State Chem.* 178 (2005) 3210.
- [28] S.T. Shishiyanu, O.I. Lupan, T.S. Shishiyanu, V.P. Şontea, S.K. Railean, *Electrochim. Acta* 49 (2004) 4433.
- [29] O. Lupan, *Technology of oxides ZnO, Cu<sub>2</sub>O, SiO<sub>2</sub> obtaining with rapid photon annealing for semiconductor devices*, Ph.D. dissertation, Technical University of Moldova, Chisinau, Moldova, 2005, 152 pp., [http://www.cnaa.acad.md/files/theses/2005/2063/oleg\\_lupan.thesis.pdf](http://www.cnaa.acad.md/files/theses/2005/2063/oleg_lupan.thesis.pdf).
- [30] S.T. Shishiyanu, O.I. Lupan, E. Monaico, V.V. Ursaki, T.S. Shishiyanu, I.M. Tiginyanu, *Thin Solid Films* 488 (2005) 15.
- [31] Joint Committee on Powder Diffraction Standards, *Powder Diffraction File No. 36-1451*.
- [32] U. Alver, T. Kılınc, E. Bacaksız, T. Küçükömeroğlu, S. Nezir, İ.H. Mutlu, F. Aslan, *Thin Solid Films* 515 (2007) 3448; B.D. Cullity, S. Rstock, *Elements of X-Ray Diffraction*, Prentice Hall, New Jersey, 2001, p. 619.
- [33] T. Mahalingam, K.M. Lee, K.H. Park, S. Lee, Y. Ahn, J.Y. Park, K.H. Koh, *Nanotechnology* 18 (2007) 035606.
- [34] A. Dev, S. Kar, S. Chakrabarty, S. Chaudhuri, *Nanotechnology* 17 (2006) 1533.
- [35] S. Kar, A. Dev, S. Chakrabarty, S. Chaudhuri, *J. Phys. Chem. B* 110 (2006) 17848.
- [36] L. Vayssieres, *Adv. Mater.* 15 (5) (2003) 464.
- [37] L. Guo, Y. Ji, *Am. Chem. Soc.* 124 (2002) 14864.
- [38] J.M. Calleja, M. Cardona, *Phys. Rev. B* 16 (1977) 3753.
- [39] H.C. Hsu, H.M. Cheng, C.Y. Wu, H.S. Huang, Y.C. Lee, W.F. Hsieh, *Nanotechnology* 17 (2006) 1404.
- [40] T.C. Damen, S.P.S. Porto, B. Tell Phys. Rev. 142 (1966) 570.
- [41] Z. Li, Y. Xiong, Y. Xie, *Nanotechnology* 16 (2005) 2303.
- [42] Y.J. Xing, Z.H. Xi, Z.Q. Xue, X.D. Zhang, J.H. Song, R.M. Wang, J. Xu, Y. Song, S.L. Zhang, D.P. Yu, *Appl. Phys. Lett.* 83 (2003) 1689.
- [43] K. Vanheusden, W.L. Warren, C.H. Seager, D.R. Tallant, J.A. Voigt, B.E. Gnade, *J. Appl. Phys.* 79 (1996) 7983.

- [44] L.S. Dake, D.R. Baer, J.M. Zachara, *Surf. Interface Anal.* 14 (1989) 71.
- [45] L.G. Mar, P.Y. Timbrell, R.N. Lamb, *Thin Solid Films* 223 (1993) 341.
- [46] V. Nefedov, J. *Electron Spectrosc. Relat. Phenom.* 25 (1982) 29.
- [47] C. Battistoni, J.L. Dormann, D. Fiorani, E. Paparazzo, S. Viticoli, *Solid State Commun.* 39 (1981) 581.
- [48] A. Pashutski, M. Folman, *Surf. Sci.* 216 (1989) 395.
- [49] P.D. Schulze, S.L. Shaffer, R.L. Hance, D.L. Utley, *J. Vac. Sci. Technol. A* 1 (1983) 97.
- [50] M. Lundholm, H. Siegbahn, S. Holmberg, M. Arbman, J. *Electron Spectrosc. Relat. Phenom.* 40 (1986) 163.
- [51] C.D. Wagner, D.E. Passoja, H.F. Hillery, T.G. Kinisky, H.A. Six, W.T. Jansen, J.A. Taylor, *J. Vac. Sci. Technol.* 21 (1982) 933.
- [52] M.A. Hartley, J.N. Chiang, D.W. Hess, D.S. Soane, *Appl. Phys. Lett.* 54 (1989) 1510.
- [53] F. Säuberlich, J. Fritsche, R. Hunger, A. Klein, *Thin Solid Films* 431–432 (2003) 378.
- [54] O. Lupan, G. Chai, L. Chow, Fabrication of ZnO nanorod-based hydrogen gas sensor, *Microelectron. J.*, in press, doi:10.1016/j.mejo.2007.09.004.